Publ. Astron. Obs. Belgrade No. 104 (2024), 125 - 132 *Invited Lecture*
https://doi.org/10.69646/aob104p125

PROPERTIES OF THE TIDAL SUBSTRUCTURES IN THE ANDROMEDA GALAXY

STANISLAV MILOŠEVIĆ

Department of Astronomy, Faculty of Mathematics,
Studentski trg 16, 11000 Belgrade, Serbia
E–mail: stanislav.milosevic@matf.bg.ac.rs

Abstract. We investigate the properties of the Giant Stellar Stream (GSS), formed in the merger of Andromeda galaxy (M31) and dwarf galaxy, the satellite of M31. We used N-body simulations to explain the properties of tidal substructures. The orientation of the GSS, distances, and velocities from our simulation are in agreement with the observed one. We confirmed that the Northeast shelf (NE) and West shelf (W) were formed in the same merger event. For the first time, we explained the observed metallicity distribution in the GSS and shell system. With a linearly decreasing gradient of the initial metallicity in the dwarf galaxy before the merger, using Monte Carlo (MC) simulations, we successfully explained the observed metallicity distribution in these substructures. These results are a contribution to the investigation of metallicity gradients in dwarf galaxies which is important for galaxy evolution in general.

1. INTRODUCTION

Galaxy mergers play an important role in galactic dynamics and evolution. In the standard hierarchical paradigm, large massive galaxies are formed in mergers of small galaxies. Andromeda (M31) is our neighboring spiral galaxy and gives us the opportunity to observe brightness profiles and measure parameters of the profiles of components of the galaxy. These measured parameters help us to describe our own Galaxy.

The Giant Stellar Stream (GSS) is discovered in the halo of M31 (Ibata et al. 2001). The GSS is a faint stellar structure formed in a merger event. This stream is spreading across ~ 6 degrees across the sky which corresponds to ~ 80 kpc (Cohen et al. 2018). The luminosity of the stream is $3.4 \times 10^7 L_\odot$, and the stellar mass $\approx 2.4 \times 10^8 M_\odot$ (Ibata et al. 2001). In the past two decades, many observations have been undertaken to determine heliocentric distances, velocities, and chemical abundances along and across the stream. In the work of McConnachie et al. (2003) are given distances along the stream in the 8 observational fields, and in Conn et al. (2016) in 19 fields. The innermost fields, those closest to M31, have contamination with M31 objects. Heliocentric velocities are given in Ibata et al. (2004), Guhathakurta et al. (2006), and Gilbert et al. (2009, 2018).

The discovery of the North Eastern and Western shelves is presented in the work of Ferguson et al. (2002). By comparing color-magnitude diagrams these structures probably have the same origin as GSS (Ferguson et al. 2005; Richardson et al. 2008). Using observations from Ferguson et al. (2002), in the work of Fardal et al. (2007) the W shelf is detected. The spectroscopic observations of the kinematics of RGB

stars in the W shelf are given in Fardal et al. (2012). The observed fields of the edges of the shells are given in Fardal et al. (2008). The edge of the NE shelf is placed on the radial distance from the center of M31 of $\approx$ 40 kpc, and the edge of the W shelf at $\approx$ 20 kpc.

Photometric and spectroscopic observations gave metallicity values of the substructures in the halo of M31. For the GSS are given metallicities along (Conn et al. 2016; Cohen et al. 2018) and across the stream (Guhathakurta et al. 2006; Kalirai et al. 2006; Ibata et al. 2007; Gilbert et al. 2009, 2014). We can see two gradients in the distribution of the observed metallicity values along the stream. Metallicity values increase from -0.7 in the inner part of the GSS, which is closest to M31, to the central part where the value is -0.2, and then in the outer part, metallicity drops off at a value around -0.8. In the direction across the stream, there is also a gradient between the central and outer part of the stream. In the study of Escala et al.(2022) it is given analyses of the metallicity and kinematics of the RGB stars in the NE shelf. The observed metallicity of the NE shelf is $[\mathrm{Fe/H}]_{\mathrm{phot}}$ = -0.42, and for the W shelf is $[\mathrm{Fe/H}]_{\mathrm{phot}}$ = -0.55.

A significant number of numerical simulations were done to explain the formation scenario of the GSS and shelves. Minor merger scenarios were investigated in the works of Fardal et al. (2006, 2007), finding good agreement between simulated and observed heliocentric distances and velocity distribution in the stream. A single-merger scenario was proposed in the work of Sadoun et al. (2014), where the turnaround radius of the satellite galaxy was 200 kpc with a null initial velocity. In Sadoun et al. (2014), a model for a satellite galaxy was introduced with a 20 times more massive dark matter halo than the baryonic part. The best time for the GSS formation was 2.7 Gyr. The position of the core of the progenitor was in the region of the NE shelf. Unlike minor merger scenarios, the major merger scenario was introduced by Hammer et al. (2010, 2013) with analyses of single and multiple mergers of M31 and its satellites. In Hammer et al. (2018) major merger scenario was also represented with hydrodynamical simulation and the mergers occurred over 2-3 Gyr, after the beginning of the simulation.

The main results of our study are presented in three papers. In Milošević et al. (2022) we investigate the metallicity gradient along the GSS. We used dSph galaxy with stellar mass $\sim 10^9 M_\odot$ as the progenitor, and with negative radial metallicity gradient explained the observed gradients along and across the GSS. In the second paper, Milošević (2022), we presented the formation of the structures in general cases when we have an M31-like galaxy and different morphologies of the progenitors. The formation of the NE and W shelves is presented in Milošević et al. (2024). With the same initial metallicity model in our progenitor, we explained the observed metallicity in the shell system.

This paper is organized as follows: in Section 2 are given N-body models of M31 and satellite galaxy, as well as the Monte Carlo method for probing initial metallicity distribution in the progenitor. In Section 3 we presented the main results, and in Section 4 the main conclusions.

2. METHODS

We generated N-body models for the M31 galaxy and dSph galaxy which is a satellite of M31. For M31 we used three main morphological components: disk, bulge, and

dark matter halo. Density profiles of these components are given in the works of Geehan (2006) and Sadoun (2014), and we use the same profiles in Milošević et al. (2022, 2024) and Milošević (2022).

For the disk, we have two profiles: exponential in the plane of the disk (x-y plane) and sech^2 law in the z-direction. The combined profile is:

$$\rho(R,z) = \frac{\Sigma(R)}{2z_0}\mathrm{sech}^2\left(\frac{z}{z_0}\right). \tag{1}$$

Here, z_0 is the scale height of the disk. The exponential profile $\Sigma(R)$ depends on the disk scale radius and the mass of the disk. The inclination of the disk is 77^o and the position angle is 37^o (Fardal et al. 2007), and the heliocentric distance to Andromeda is taken to be 785 kpc (Stanek & Garnavich, 1998).

The bulge is represented with the Prugniel-Simien profile (Widrow et al. 2008), which is a de-projected Sersic profile:

$$\rho_b = \rho_{b0}\left(\frac{r}{r_b}\right)\exp\left(r/r_b\right)^{-1/n}. \tag{2}$$

Here, ρ_{b0} is the density at $r = r_b$, and r_b is a spherical scale radius for the bulge, and the value for n is 1.8.

A spherical dark matter halo is represented with the Navarro-Frenk-White profile (Navaro et al. 1996), using its more general form (Widrow, et al. 2008):

$$\rho(r) = \frac{2^{2-\alpha}\sigma_h^2}{4\pi r_s^2}\frac{1}{(r/r_s)^\alpha(1+r/r_s)^{3-\alpha}}\frac{1}{2}\mathrm{erfc}\left(\frac{r-r_h}{\sqrt{2}\delta_{r_h}}\right). \tag{3}$$

Here, r_h is the radius of the halo and the value at which density starts to decrease, δ_{r_h} is the distance along which density falls to zero, α is an exponent in NFW profile, and we took $\alpha = 1$.

For generating initial conditions we used the GalactICs package (Widrow et al. 2008) and for the running simulation Gadget2 code (Springel, 2005). The values for the parameters in the models are given in tables in Milošević et al. (2022, 2024). We investigated several merger scenarios. For the two morphologies of the satellite galaxy: dSph and dwarf with a disk, we have undertaken several simulations with different orbit inclinations to find properties of the formed structures in general. For the formation of the GSS and shell system, a satellite galaxy started its very radial orbit with a null initial velocity from 200 kpc initial distance.

To describe metallicity distribution in the GSS we tested the linearly desreasing function for the metallicity distribution in the progenitor. Then we vary the parameters of the linear function in the progenitor and use Monte Carlo (MC) simulation to find which one produces the match between the simulated and the observed metallicity distribution in the GSS given in Conn et al. (2016) and Cohen et al. (2018). The MC procedure is described in Milošević et al. (2022).

3. RESULTS

We present two groups of results: formation and kinematical properties of the GSS and shell system, and metallicity distribution in these structures. Figure 1 presents the formation of the GSS, NE, and W shelf after 2.4 Gyrs from the beginning of the simulation. We compared our simulated data with observed one from McConnachie et al. (2003) and Conn et al. (2016) and there is agreement with observations (the left panel in Figure 1). In the middle panel, we presented a surface density plot for better visibility because shells are very faint structures. In both panels are shown structures in the x-y plane, which is the plane of the sky. On the right panel are given simulated particles in the x-z plane. Here we can see that the NE shelf is formed closer to us due to M31, and the GSS and W shelf further away from us. The GSS is formed in the first, the NE shelf in the second, and the W shelf in the third pericentric passage of the satellite galaxy. The distances and velocities along the stream are presented in Figure 2 and Figure 3. In Figure 2 we can see agreement in all fields along the stream between simulated distances and observed one from McConachie et al. (2003) and Conn et al. (2016). We compared results from our simulation in the time interval from 2 to 3.5 Gyrs, as it is suggested from previous studies that this is the best timescale for halo substructure formation in M31 (Sadoun et al. 2014; Hammer et al. 2018).

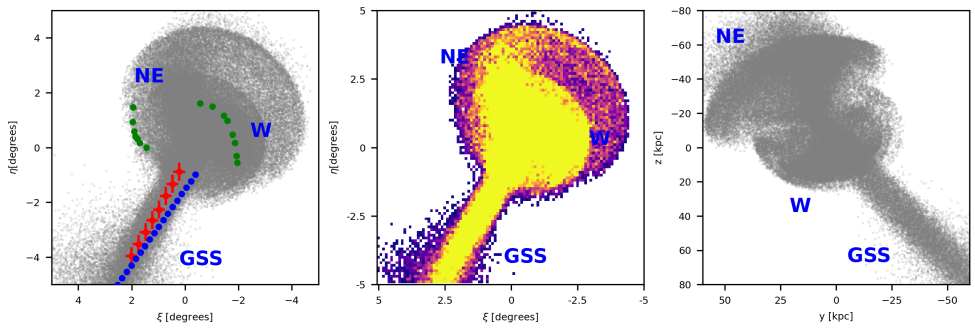

Figure 1: The GSS, NE, and W shelves after 2.4 Gyrs. Red crosses are the observed fields given in McConnachie et al. (2003), blue dots in Conn et al. (2016), and green dots are the edges of the NE and W shelves given in Fardal et al. (2008). Observed fields for the NE shelf from Escala et al. (2022) are given in black dots and also for the W shelf from Fardal et al. (2012). The figure is from Milošević et al. (2024).

With the MC method, we tested linearly decreasing function for the initial metallicity in the progenitor galaxy. In Figure 4 we present results from these simulations. On the particles in the progenitor, we attach metallicity values trace them through the simulation and then calculate metallicity values in the fields that correspond to the observed one in Conn et al. (2016). In these 19 fields, we compared simulated and observed metallicities from 2.2 to 3 Gyrs. We found the best agreement for the 2.9 Gyrs.

Stellar shells are very faint structures and it can be better seen in phase-space plots where radial distance is on x-axes and radial velocity on y-axes. In Figure 5 are presented formed structures in the merger event of M31 and its satellite. We can see two shells and the GSS. For comparison with observation, we presented our results in

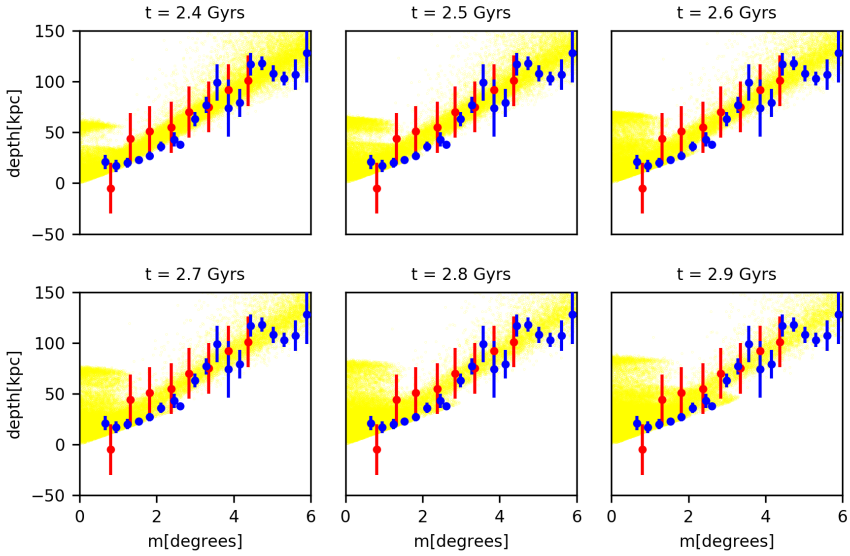

Figure 2: Distances from the center of M31 on the y-axis. Red bars are observed values for stars from McConnachie et al. (2003), and blue Conn et al. (2016). Dots are simulated particle distances in our N-body simulation. Panels show different moments into the merger, from 2.4 to 2.9 Gyrs. The figure is from Milošević et al. (2022).

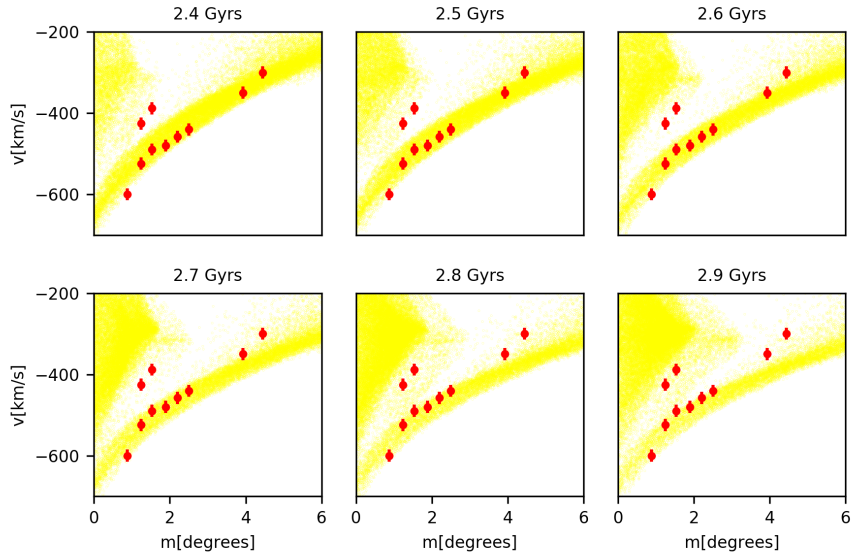

Figure 3: Radial velocities along the GSS as a function of distance for the time interval between 2.4 and 2.9 Gyrs. Over-plotted thick red dots are the observed values from Ibata et al. (2004), Guhathakurta et al. (2006), and Gilbert et al. (2009). The figure is from Milošević et al. (2022).

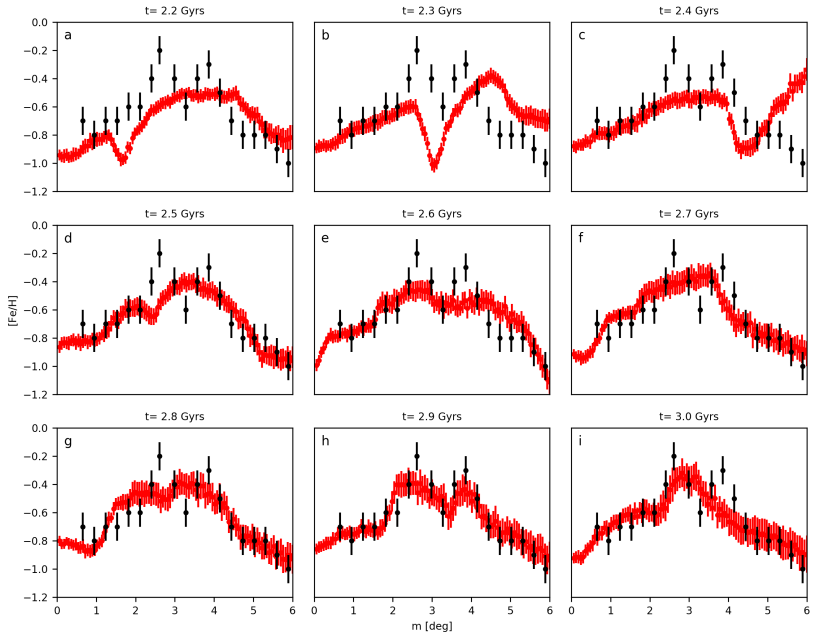

Figure 4: Metallicity distribution along the stream from 2.2 Gyrs to 3.0 Gyrs. Red dots with error bars represent metallicity from MC simulation and black dots are results given by Conn et al. (2016). The figure is from Milošević et al. (2022).

$R_{proj} - v_{los}$ space. In Figure 6 we have a typical wedge pattern for structures formed in radial mergers, such as shells. The edge of the NE shelf is 40 kpc from the center of M31. For the formation of the NE shelf, the best timescale is 2.4 Gyrs, due to the position of the tip of the wedge pattern. From different criteria, the timescale for forming the structures in the halo of M31 is between 2.4 and 2.9 Gyrs.

4. SUMMARY

We used the dSph model for the progenitor galaxy to explain the formation of the structures in the halo of M31. These structures are formed in the merger event of M31 and its satellite. The most prominent structure is the GSS. The stream is formed in the first pericentric passage, and in the second is formed the NE shelf, in the third the W shelf.

Our model successfully reproduces properties of the GSS. We compare the orientation of the stream, distances, and velocity distribution with observations from McConnachie et al (2003), Conn et al. (2016), for distances and Ibata et al. (2004), Guthatakurta et al. (2006), Gilbert et al. (2009) for velocities and found an agreement.

We used a linearly decreasing function for the initial metallicity distribution in the progenitor to explain the observed metallicity distribution in the stream given in Conn et al. (2016) and Cohen et al. (2018). With negative metallicity gradient: Δ[Fe/H] = -0.3 $\pm$ 0.2 we explained metallicity distribution along and across the

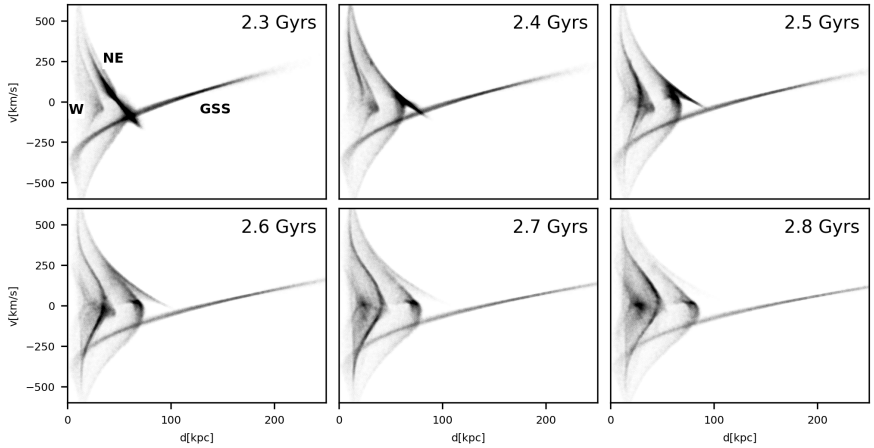

Figure 5: The phase-space plots in $d - v_r$ for different timescales between 2.3 and 2.8 Gyrs. We can see the evolution of the tidal structures: GSS, NE, and W shelves on this time interval. The figure is from Milošević et al. (2024).

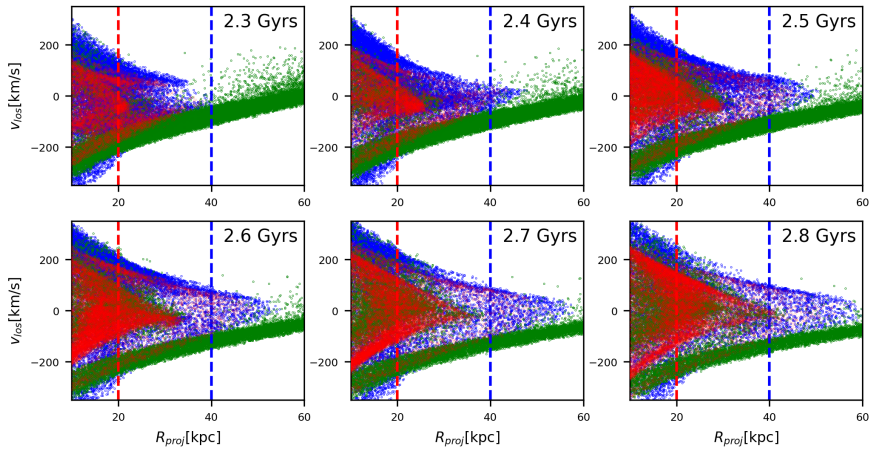

Figure 6: The density plot in $R_{proj} - v_{los}$ plane from 2.3 to 2.8 Gyrs. With green color are presented particles from the GSS; with blue the NE shelf, and with red the W shelf. Red and blue dashed lines present suggested positions of the observed tip of the wedge pattern for the W and NE shelves, respectively. The figure is from Milošević et al. (2024).

stream. Two peaks in the central part of the metallicity distribution along the stream are explained with a complex kinematical picture where we have at least two groups of objects that are moving in opposite directions and make these peaks a temporary structure. The results are presented in Milošević et al. (2022), Milošević (2022), and Milošević et al. (2024).

Using the same N-body model and the model for initial metallicity we compared simulated values from the NE and W shelves with observed properties given in Escala et al. (2022). We reproduced mean metallicity values in the shell system. The

formation of the shells occurred in the same merger event, where a satellite galaxy on a very radial orbit passes several times near the center of M31.

Acknowledgements

This work was supported by the Ministry of Science, Technological Development and Innovation of the Republic of Serbia, through contracts: no. 451-03-66/2024-03/200104 and no. 451-03-66/2024-03/200002.

References

Cohen R. E., Kalirai J. S., Gilbert K. M., Guhathakurta P., et al.: 2018, *ApJ*, **156**, 230
Conn A. R., McMonigal B., Bate N. F., et al.: 2016, *MNRAS* , **458**, 3282
Escala I., Gilbert K. M., Fardal M., Guhathakurta P., et al.: 2022, *AJ*, **164**, 20
Fardal M. A., Babul A., Geehan J. J., Guhathakurta P.: 2006, *MNRAS*, **366**, 1012
Fardal M. A., Guhathakurta P., Babul A., McConnachie A. W.: 2007, *MNRAS*, **380**, 15
Fardal M. A., Babul A., Guhathakurta P., Gilbert K. M., Dodge C.: 2008, *ApJ*, **682**, L33
Fardal M. A., et al.: 2012, *MNRAS*, **423**, 3134
Ferguson A. M. N., Irwin M. J., Ibata R. A., Lewis G. F., Tanvir N. R.: 2002, *AJ*, **124**, 1452
Ferguson A. M. N., Johnson R. A., Faria D. C., Irwin M. J., et al.: 2005, *ApJ*, **622**, L109
Geehan J. J., Fardal M. A., Babul A., Guhathakurta P.: 2006a, *MNRAS*, **366**, 996
Gilbert K. M., Guhathakurta P., Kollipara P., et al.: 2009, *ApJ*, **705**, 1275
Gilbert K. M., Kalirai J. S., Guhathakurta P., et al.: 2014, *ApJ*, **796**, 76
Gilbert K. M., Tollerud E., Beaton R. L., et al.: 2018, *ApJ*, **852**, 128
Guhathakurta P., Rich R. M., Reitzel D. B., et al.: 2006, *AJ*, **131**, 2497
Hammer F., Yang Y. B., Wang J. L., et al.: 2010, *ApJ*, **725**, 542
Hammer F., Yang Y. B., Fouquet S., et al.: 2013, *MNRAS*, **431**, 3543
Hammer F., Yang Y. B., Wang J. L., et al.: 2018, *MNRAS*, **475**, 2754
Ibata R., Irwin M., Lewis G., Ferguson A. M. N., Tanvir N.: 2001, *Nature*, **412**, 49
Ibata R., Chapman S., Ferguson A. M. N., Irwin M., Lewis G.: 2004, *MNRAS*, **351**, 117
Ibata R., Martin N., Irwin M., et al.: 2007, *ApJ*, **671**, 1591
Kalirai J. S., Guhathakurta P., Gilbert K. M., et al.: 2006, *ApJ*, **641**, 268
McConnachie A. W., Irwin M. J., Ibata R. A., et al.: 2003, *MNRAS*, **343**, 1355
Milošević S.: 2022, *SerAJ*, **205**, 33
Milošević S., Mićić M., Lewis G. F.: 2022, *MNRAS*, **511**, 2868
Milošević S., Mićić M., Lewis G. F.: 2024, *MNRAS*, **527**, 4797
Navarro J. F., Frenk C. S., White S. D. M.: 1996, *ApJ*, **462**, 563
Richardson J. C., et al.: 2008, *AJ*, **135**, 1998
Sadoun R., Mohayaee R., Colin J.: 2014, *MNRAS*, **442**, 160
Springel V.: 2005, *MNRAS*, **364**, 1105
Stanek K. Z., Garnavich P. M.: 1998, *ApJ*, **503**, L131
Widrow L. M., Pym B., Dubinski J.: 2008, *ApJ*, **679**, 1239